

# **TES carbon monoxide validation with DACOM aircraft measurements during INTEX-B 2006**

M. Luo<sup>1</sup>, C. Rinsland<sup>2</sup>, B. Fisher<sup>1</sup>, G. Sachse<sup>3</sup>, G. Diskin<sup>3</sup>, J. Logan<sup>4</sup>, H. Worden<sup>1</sup>, S. Kulawik<sup>1</sup>, G. Osterman<sup>1</sup>, A. Eldering<sup>1</sup>, R. Herman<sup>1</sup> and M. Shephard<sup>5</sup>

**Revision  
July 26, 2007**

<sup>1</sup> Jet Propulsion Laboratory  
California Institute of Technology  
4800 Oak Grove Drive  
Pasadena, CA 91109 U.S.A.

<sup>2</sup> NASA Langley Research Center  
Mail Stop 401A  
Hampton, VA 23681-2199 U.S.A.

<sup>3</sup> NASA Langley Research Center  
Mail Stop 483  
Hampton, VA 23681-2199 U.S.A.

<sup>4</sup> Division of Engineering and Applied Sciences  
Harvard University  
Cambridge, MA 02138 U.S.A.

<sup>5</sup> Atmospheric and Environmental Research, Inc.  
Lexington, MA 02421 U.S.A.

1 **Abstract**

2

3 Validation of TES (Tropospheric Emission Spectrometer) tropospheric CO profiles with  
4 *in-situ* CO measurements from the DACOM (Differential Absorption CO Measurement)  
5 instrument during the INTEX (Intercontinental Chemical Transport Experiment)-B  
6 campaigns in March-May 2006 are presented. For each identified DACOM CO profile,  
7 one to three TES CO profiles are selected closest in location to the small area that the  
8 DACOM profile covers. The time differences between the comparison profiles are  
9 within two hours. The DACOM CO vertical profiles are adjusted by applying nearest  
10 coincident TES averaging kernels and the *a priori* profiles. This step accounts for the  
11 effect of the vertical resolution of the TES CO retrievals and removes the influence of the  
12 *a priori* assumptions in the comparisons. Comparison statistics for data taken near  
13 Houston in March 2006 show good agreement between TES and the adjusted DACOM  
14 CO profiles in the lower and mid-troposphere with a correlation coefficient of 0.87. On  
15 average, the TES CO volume mixing ratio profile is 0-10% lower than the adjusted  
16 DACOM CO profile from the lower to middle troposphere. This is within the 10-20%  
17 standard deviations of the TES or DACOM CO profiles taken in the Houston area. The  
18 comparisons of TES and DACOM CO profiles near Hawaii and Anchorage in April-May  
19 2006 are not as good. In these regions, the aircraft DACOM CO profiles are  
20 characterized by plumes or enhanced CO layers, consistent with known features in the  
21 tracer fields due to transpacific transport of polluted air parcels originating from East  
22 Asia. Although TES observations over the Pacific region also show localized regions of  
23 enhanced CO, the coincidence criteria for obtaining good comparisons with aircraft  
24 measurements are challenging. The meaning of validation comparisons in profile  
25 portions where TES retrievals have little sensitivity is addressed. Examinations of  
26 characteristic parameters in TES retrievals are important in data applications.

## 27 1. Introduction

28

29 The TES instrument on the NASA Aura satellite has been making nadir measurements of  
30 the Earth infrared spectral radiance since September 2004 [Beer *et al.*, 2001; Beer, 2006].

31 TES retrievals of co-located tropospheric ozone and CO profiles from the radiance  
32 measurements are key products for studies of ozone chemistry and transport in the  
33 troposphere. Validation efforts for TES ozone and CO profiles have been documented  
34 and updated *via* the TES Validation Report [Osterman *et al.*, 2006] and publications [e.g.  
35 Worden *et al.*, 2007; Nassar *et al.*, this issue]. In addition, Rinsland *et al.* [2006]  
36 presented the historical trends of the TES instrument performance and the associated  
37 trends for the sensitivities in TES-retrieved CO profiles. Luo *et al.* [2007] presented  
38 comparisons of TES CO retrievals and those from MOPITT and addressed the issues of  
39 proper comparisons between remote sensing retrievals. Several aircraft campaigns have  
40 been conducted that have produced data for Aura instrument validation, *e. g.*, AVE (Aura  
41 Validation Experiment) near Houston in Oct-Nov 2004, Costa Rica AVE in Jan-Feb  
42 2006, and INTEX-B in March-May 2006 near Houston, TX, Hawaii, HI, and Anchorage,  
43 AK. This paper describes the TES CO validations using *in-situ* CO measurements by the  
44 DACOM instrument [Sachse *et al.*, 1987] on the DC-8 aircraft during the INTEX-B  
45 campaign (<http://www.espo.nasa.gov/intex-b/>). The validation of TES CO data using  
46 measurements from the AVE campaigns are presented by Lopez *et al.* [2007] of this  
47 special issue.

48

49 Aircraft *in-situ* measurements of atmospheric specie concentrations can be useful in  
50 validating retrievals from the satellite remote sensing measurements (*e. g.*, Emmons *et*  
51 *al.*, 2004). However, there are some challenges in performing these comparisons. First,  
52 only a very limited number of comparison pairs can be obtained over coincident pressure  
53 ranges, locations and times. As a tracer of atmospheric transport with a lifetime of weeks  
54 [Logan *et al.*, 1981], the CO distribution has distinct characteristics associated with  
55 sources and meteorological conditions in different areas. It is therefore difficult to fully  
56 address possible systematic biases in the two measurement sets. The second difficulty is  
57 that in the process of proper comparison, the *in-situ* high vertical resolution

58 measurements need to be adjusted by the remote sensing observation operators including  
59 *a priori* assumptions used in the satellite data retrievals. As clouds are common in the  
60 troposphere, their presence is also an important factor to consider when comparing space-  
61 based measurements with *in-situ* measurements. Validation comparisons are therefore  
62 only performed for satellite retrievals sensitive to the nadir radiance measurements. In  
63 low sensitivity cases where *a priori* dominates the retrieval profiles, the comparison is  
64 meaningless. We illustrate the above points with TES CO data validation in the three  
65 phases of the INTEX-B campaign.

66

67 TES nadir retrievals of CO in the middle to upper troposphere are compared with  
68 retrievals from limb measurements made with MLS (Microwave Limb Sounder)  
69 instruments (*Livesey et al.*, this issue). TES CO validation using the Argus and Alias *in-*  
70 *situ* measurements in the AVE campaigns and the comparisons between the two *in-situ*  
71 results are documented in a separate paper (*Lopez et al.*, this issue). We will discuss  
72 future TES CO validation activities with larger data sets at the conclusion of this paper.

73

74

## 75 **2. TES and DACOM observations of CO during INTEX-B 2006**

76

77 During INTEX-B 2006, TES made routine Global Survey (GS) measurements every  
78 other day, and scheduled Step & Stare (SS) special observations in the GS ‘off’ days over  
79 the regions where the aircraft flew. TES nadir footprints are separated by ~180 km along  
80 the Aura ground track for GS and ~45 km for SS observations. The size of a TES nadir  
81 footprint is about 5 km X 8 km. Figures 1 and 2 illustrate TES measurement locations  
82 and the CO values at 681.3 hPa near Houston in March 11-26 (16 days) and over  
83 northern Pacific Ocean in April 19-23 (4 days). TES measurements of CO in both areas  
84 show day-to-day variability depending on the strength of the CO sources, the  
85 meteorological conditions, and the TES measurement locations and times. In general,  
86 the CO distributions in the three INTEX-B areas show different characteristics. For  
87 example, compared to the Houston area, CO values near Hawaii and Anchorage show

88 larger variations in the middle or upper troposphere associated with episodes of  
89 transpacific transport of polluted air.

90

91 This paper uses TES Version 003 data that have been recently processed and were  
92 available for only a few TES observation days at the time of this paper was written. The  
93 major difference between V003 and V002 for the TES CO retrievals is the increased  
94 variability at high latitudes due to a relaxation of the retrieval constraint.

95

96 For TES CO validation, we group the DACOM CO measurements into three groups:  
97 Houston, Hawaii, and Anchorage. During the INTEX-B campaign, the flight planning  
98 teams made efforts to schedule parts of the aircraft flight path along a portion of the Aura  
99 ground track with the aircrafts flew both ascending and descending spirals near TES  
100 footprints to optimize the profile samplings for validation of the TES profiles. Figures 3,  
101 4, and 5 illustrate the DC-8 flight paths and the TES nadir measurement locations for  
102 three days during the INTEX-B campaign. Vertical profiles are identified for each flight  
103 in the figures. The flight path for each day is unique and details can be found on the  
104 INTEX-B website [<http://www.espo.nasa.gov/intex-b/>]. During these flights there were 9  
105 DC-8 profiles near Houston, 13 profiles near Hawaii, and 3 profiles near Anchorage  
106 which can be used for TES and DACOM CO comparisons.

107

108 Tables 1, 2, and 3 provide more detail about the TES-DACOM comparisons. Up to three  
109 TES profiles are selected close in location to each DACOM profile. For each comparison  
110 the distance and the time between TES and DACOM profiles are recorded. Most  
111 comparisons are within two hours and 100 km.

112

113 TES CO retrievals have been described previously by Rinsland et al. [2006] and Luo et  
114 al. [2007]. In particular, the vertical resolution of the CO retrievals and the influence of  
115 the *a priori* assumptions on the retrievals are characterized by the degrees of freedom for  
116 signal (DOF). In cases where clouds were in the field of view, TES CO retrievals under  
117 the clouds are dominated by the *a priori*. As illustrated in the next section, the TES CO  
118 averaging kernel describes the vertical extent to which the true CO profile contributes to

119 each of the retrieved values. Table 1-3 also list DOFs and the effective cloud optical  
120 depths (OD) [Kulawik *et al.*, 2007] for the selected TES CO profiles paired with  
121 DACOM CO profiles. For most cases, the effective cloud OD retrieved by TES is less  
122 than 0.1, and the DOF for most cases are greater than 1.2.

123

124 Many of the INTEX-B aircraft flights were scheduled to coincide with TES Step & Stare  
125 (SS) observations. Figure 6 is an example of TES CO retrievals along the Aura flight  
126 track plotted as a cross-section of latitude vs. pressure on March 4, 2006. The TES SS  
127 covers South America, the Caribbean Sea, the Gulf of Mexico, and extends to the north  
128 across Mississippi etc. The enhanced CO in the lower troposphere is evident over S.  
129 America (5S-10N), the Gulf of Mexico (20N-30N), and the continental United States  
130 (30N-45N). The flight path of the DC-8 is overlaid on the TES CO curtain image. It  
131 sampled a very limited portion of the atmosphere that the TES SS covered.

132

133 The DACOM spectrometer system is an airborne fast-response (1 sec) high precision (1%  
134 or 1 ppbv) sensor that includes three tunable diode lasers providing 4.7, 4.5 and 3.3  $\mu\text{m}$   
135 radiation for accessing CO, N<sub>2</sub>O, and CH<sub>4</sub> absorption lines respectively [Sachse *et al.*,  
136 1987]. Calibration for all species is accomplished by periodically (~ every 10 minutes)  
137 flowing calibration gas through this instrument. By interpolating between these  
138 calibrations, slow drifts in instrument response are effectively suppressed yielding high  
139 precision values. Measurement accuracy is closely tied to the accuracy of reference gases  
140 obtained from NOAA/CMDL, Boulder, CO. Figure 7 shows DACOM CO measurements  
141 for the flight of March 4, 2006. A qualitative comparison between the TES CO latitude  
142 vs. pressure (Figure 6) cross-section and the DACOM measurements in the right-bottom  
143 panel of Figure 7 shows reasonable agreement, e.g., high CO near the surface. Another  
144 way to illustrate this qualitative comparison is displaying the TES CO volume mixing  
145 ratios sampled along the DACOM flight track. In this comparison, linear interpolations  
146 of CO values over pressure and latitude are performed. Figure 8 shows the sampled TES  
147 CO and the DACOM CO comparisons along the DC-8 flight track for the March 4<sup>th</sup>  
148 flight. As the DC-8 flew to higher and lower altitudes, changes in TES CO mixing ratios  
149 are similar to those measured by DACOM.. The peak-to-peak changes in CO for TES

150 are less than that of DACOM due to the vertical smoothing effect in nadir remote sensing  
151 retrievals, which is discussed in the next section.

152

153

### 154 **3. CO profile comparisons between TES nadir retrievals and DACOM** 155 ***in-situ* measurements**

156

157 For each identified *in-situ* CO profile, 1 to 3 TES CO profiles closest in distance to the  
158 DACOM locations are identified. As an example, the latitude marks in the right-bottom  
159 panel of Figure 7 show the latitudes of the selected four TES CO profiles, where the  
160 black mark is the one closest to the averaged DACOM locations.

161

162 Figures 9 and 10 illustrate steps taken in the TES-DACOM comparisons. Figure 9 is for  
163 the March 4, 2006 flight near Houston (~50 km and ~1 hr between TES and DACOM  
164 profiles) and Figure 10 is for the April 28, 2006 flight near Hawaii (~6 km and 1.5-2 hr  
165 between TES and DACOM profiles). The upper-left panels show the original DACOM  
166 CO profile and the nearby TES profiles with retrieval errors. Although each DACOM  
167 CO profile derived from an aircraft vertical samplings is unique with layers of enhanced  
168 CO, the scales and vertical extends of the anomalous CO layers near Houston are  
169 generally small compared to those taken in Hawaii and Anchorage area. Furthermore,  
170 most of the elevated DACOM CO layers in the Houston area are found near the surface  
171 while the elevated DACOM CO layers in Hawaii/Anchorage regions are mostly in the  
172 middle-to-upper troposphere. The comparisons in Figure 9 show that the TES and  
173 DACOM CO profiles have a similar shape, with the DACOM observations having more  
174 vertical structure (resolution). . In Figure 10, the TES retrieved CO profile departed from  
175 the initial (*a priori*) profile towards the DACOM profile but does not compare well with  
176 the *in-situ* profile in the lower and middle troposphere.

177

178 The DACOM *in-situ* measurement of CO has a vertical resolution much higher than that  
179 of TES and therefore direct comparisons between the two can be misleading. The remote  
180 sensing retrievals work by optimally combining the information from the spectral

181 measurements and the *a priori* state of the CO profile using reasonable constraints. The  
182 retrieved species profile,  $x_{ret}$ , can be related to the true profile,  $x$ , by the following  
183 equation [Rodgers, 2000]:

184

$$185 \quad x_{ret} = Ax + (I - A)x_a + \varepsilon \quad (1)$$

186 where  $A$  is the averaging kernel matrix,  $x_a$  is the *a priori* profile, and  $\varepsilon$  is the retrieval  
187 error due to random errors in the measurement and the systematic errors in the forward  
188 model. The averaging kernels are the key to understanding the satellite retrievals. The  
189 right-upper panel of Figure 9 and 10 show examples of TES averaging kernels at three  
190 selected pressure levels of lower, middle and upper troposphere. The TES-retrieved CO  
191 profile is the combination of vertically smoothed true profile (1<sup>st</sup> term of equation 1) and  
192 the *a priori* profile weighted by  $(I-A)$ , the 2<sup>nd</sup> term of equation (1).

193

194 For satellite data validation purposes, the high vertical resolution *in-situ* measured CO  
195 profile with high precision can be treated as the true profile,  $x$ . For example, a DACOM  
196 CO profile measured during a downward spiral has over 1000 measurement points. The  
197 direct comparison of the TES-retrieved CO profile,  $x_{ret}$  to the DACOM CO profile,  $x$ , is  
198 then not meaningful due to their different vertical resolutions. In order to compare the *in-*  
199 *situ* and the retrieved profiles properly, the *in-situ* profile ( $x$ ) must be converted to  $x_{ret}$  via  
200 Equation (1) and then compare this adjusted profile to the satellite retrieved profile  
201 (Rodgers and Connor, 2003; Emmons *et al.*, 2004; Luo *et al.*, 2007).

202

203 It is important to point out that the *in-situ* CO profile can only be used to evaluate the  
204 TES CO retrievals where the TES spectral measurements are sensitive to the  
205 perturbations of the CO values. Profiles of CO retrieved by TES and all other infrared  
206 sounders differ from those from an ideal instrument in that they are smoothed by the *a*  
207 *priori* constraints applied in the retrieval process. The *in-situ* CO measurement (viewed  
208 as the true CO profiles in satellite data validation) will not be able to justify the absolute  
209 TES CO retrieval values. In the processing of applying Equation (1) to the *in-situ*  
210 DACOM CO profiles, we add the influence of the TES *a priori* constraints. When we

211 compare these adjusted *in-situ* CO profiles to the TES retrievals, the effect of *a priori* is  
212 canceled out.

213 The bottom two panels of Figure 9 show adjusted DACOM CO profiles compared to the  
214 TES CO profiles and their differences for the March 4, 2006 flight. Since the DACOM  
215 profile only covers below about 200 hPa, we use shifted TES *a priori* profile to extend  
216 the DACOM profile to above this pressure level before applying the TES averaging  
217 kernel to it in Equation (1). The TES CO *a priori* profile and its comparison to the  
218 DACOM profile are also shown in Figure 9 as reference. In this comparison, TES CO  
219 profiles show a larger vertical decrease with altitude than the DACOM profile.

220 In the case of Figure 10 (April 28, near Hawaii), the TES CO retrievals do not show the  
221 layer of enhanced CO in 500-250 hPa that DACOM detected, which is also an evident in  
222 the adjusted DACOM CO profile. Studies show that Asian air pollution outflow and its  
223 transpacific transport are characterized by sporadic events of high CO in the central and  
224 northern pacific in spring [Heald *et al.*, 2003]. This characteristic is seen in TES CO  
225 global survey observations as high variability between adjacent profiles along an  
226 orbit[Rinsland *et al.*, 2006]. These sporadic events make validation of the CO profile  
227 more difficult, compared to those from regions with more homogeneous CO.

228

229

#### 230 **4. Comparison statistics for the three INTEX-B areas**

231

232 The comparison statistics between TES CO retrievals and DACOM measurements are  
233 compiled separately for the three INTEX-B time periods. Houston, Hawaii, and  
234 Anchorage are all affected by different CO production sources and transport mechanisms.  
235 During the spring season, March – May, the tropics biomass burning sources of CO in  
236 South America and Africa are at their annual minimum so their influence to the INTEX-  
237 B observation regions is negligible. TES and MOPITT CO global distributions show  
238 higher CO in northern high latitudes with identifiable sources over China (Clerbaux *et*  
239 *al.*, 2004, Rinsland *et al.*, 2006; Luo *et al.*, 2006). By comparison, the CO values in  
240 Houston area are more uniform and smaller in magnitude. Therefore, the measurements

241 of CO made by TES and DACOM reflect the different characteristics of the three  
242 regions.

243

244 The averaging kernels for a given satellite retrieved profile are the key for understanding  
245 the physics in the process as illustrated in Figure 9 and 10 for the two example cases.

246 They describe how sensitive that the retrieved value at a given pressure level to the true  
247 species values at all levels. The areas of the averaging kernels represent the fractions of  
248 the contributions of the true profile to the retrievals as a function of pressure [Rodgers,  
249 2000]. Figure 11 shows the profiles of the TES CO averaging kernel areas in Houston,  
250 Hawaii, and Anchorage regions, respectively. TES CO retrieved profiles are most  
251 sensitive in the pressure regions below 200 hPa and above ~700 hPa for the Houston  
252 region and 600-550 hPa in Hawaii and Anchorage regions. TES CO profiles are less  
253 sensitive to the true state in the lower and upper troposphere, and the retrievals in these  
254 pressure ranges are dominated by the a priori

255

256 Figure 12 shows the summary comparisons between TES and DACOM CO profiles near  
257 Houston, March 2006. The correlation coefficient for all selected TES and DACOM CO  
258 profiles is 0.87, and improves to 0.94 when only one TES CO profile closest to the  
259 averaged DACOM location is considered for a given DACOM CO profile. The  
260 agreement between TES and DACOM CO profiles is within 10% in the lower and middle  
261 troposphere with TES being lower in the mid-troposphere. The difference between TES  
262 and DACOM CO observations is smaller than the variability of both the TES and  
263 DACOM measurements for this region. The standard deviations of TES and DACOM  
264 CO data are 10-15% and 15-20% respectively. The standard deviations of TES CO  
265 retrievals are comparable with the estimated total errors in TES retrievals. The TES CO  
266 observation errors, including errors due to measurement noise and the systematic errors  
267 (the last term in Equation 1) should be the error associated with TES and DACOM CO  
268 data comparisons here if the variability due to offsets in time and location are ignored  
269 [Rodgers and Connor, 2003]. The TES observation error is estimated to be 5-10% in the  
270 low-mid latitudes [Rinsland *et al.*, 2006].

271

272 Figure 13 shows the summary comparisons between TES and DACOM CO profiles near  
273 Hawaii, April-May 2006. The data correlation coefficient is only 0.23 (not shown). The  
274 DACOM CO profiles in this area showed larger variability (see the example in Figure 10)  
275 compared to those taken in Houston area. In most flights, DACOM CO profiles detected  
276 plumes or enhanced CO layers in mid-troposphere (daily report in  
277 <http://www.espo.nasa.gov/intex-b/>). In these situations the CO concentrations vary  
278 strongly with location and time, thus a slight mismatch between the TES and DACOM  
279 CO profiles could result in substantial differences. The selected TES retrieved CO  
280 profiles do not capture the broad layers of enhanced CO in the adjusted DACOM  
281 profiles, but most of them have moved away from the initial guess to either match the  
282 shapes or the magnitudes of the *in-situ* profiles to some degree.

283

284 Figure 14 shows the summary comparisons between TES and DACOM CO profiles near  
285 Anchorage, May 2006. The average of the three adjusted DACOM CO profiles shows a  
286 huge enhancement of CO in the middle and upper troposphere, dominated by the  
287 observations on May 7, 2006 (<http://www.espo.nasa.gov/intex-b/>). This layer of  
288 enhanced CO observed in the DACOM measurement is not captured by the TES  
289 retrievals sampled 300 km away. For the May 9 flight in which the DACOM spiral CO  
290 profile was within a few tens of kilometers from the TES profiles, but 1.5-2.0 hours apart,  
291 the three TES CO profiles still disagree with that of DACOM by +/- 35%. The  
292 meteorological conditions (<http://www.espo.nasa.gov/intex-b/>) suggest that the area is  
293 part of the transpacific pathway for the pollution events originated in the north-east  
294 China, hence comparisons between TES and the *in-situ* measurements of CO are not  
295 expected to be in good agreement.

296

297 In the portions of a given profile where TES measurements have low sensitivity to the  
298 species profile, the agreement between TES retrievals and the adjusted *in-situ*  
299 measurements is nearly perfect but is meaningless. For example, in all comparisons in  
300 the three areas, TES and DACOM CO values agree much better in the lower troposphere  
301 than the mid-troposphere (Figures 12-14). This is because TES retrievals and the  
302 adjusted DACOM CO profiles near the surface are both dominated by the *a priori*

303 assumptions (see Figure 11) due to the low sensitivity of TES measurements to this  
304 portion of the atmosphere.

305

306

## 307 **5. Conclusions**

308

309 We have presented validation of TES CO retrievals with the *in-situ* CO measurements  
310 taken by the DACOM instrument on the DC-8 during the INTEX-B aircraft campaign, in  
311 March-May 2006. Following proper procedures for comparisons between remote  
312 sensing retrievals and *in-situ* measurements, we adjusted DACOM CO profiles by the  
313 TES averaging kernels and the *a priori* profiles from the TES CO retrievals. The  
314 comparisons between TES and the adjusted DACOM CO profiles for the three INTEX-B  
315 regions, near Houston, Hawaii, and Anchorage, are representative examples of different  
316 atmospheric conditions. In the area where the background level of CO in the atmosphere  
317 dominates with relatively small contributions from regional pollution and long range  
318 transport (near Houston), the TES and the adjusted DACOM CO profiles show similar  
319 shapes and the correlation coefficient has a high value of 0.87. In the area where  
320 pollution transport dominates the CO profiles, *e. g.*, near Hawaii and Anchorage, TES  
321 and the adjusted DACOM CO profiles do not agree well and the DACOM *in-situ* CO  
322 measurements show enhanced CO layers in middle or lower troposphere sporadically. It  
323 is therefore difficult to use such data for satellite profile validation, due to highly  
324 restrictive requirements for time and location coincidences.

325

326 It should be noted that the differences reported here cannot be used to evaluate the  
327 absolute accuracy of the satellite retrieved profiles. The absolute error in the retrieved  
328 profile necessarily include additional uncertainties such as bias in TES radiances  
329 [Shephard *et al.*, 2007], errors in the spectroscopic parameters adopted for CO,  
330 systematic errors in the retrieval (e.g. clouds, temperature, etc.), and *a priori*  
331 assumptions. We have therefore focused on understanding the bias of TES  
332 measurements with respect to *in situ* profiles where the smoothing error is explicitly  
333 removed [Rodgers, 2000, Rodgers and Connor, 2003]. When using the methods

334 described in this and other papers (*e. g.*, Emmons *et al.*, 2004; Worden *et al.*, 2007, Luo  
335 *et al.*, 2007), the effect of the *a priori* profile is removed when differencing the TES  
336 retrieval and the adjusted in situ profile. In the portions of the vertical profile where TES  
337 has very little sensitivity and therefore retrieval errors are dominated by the smoothing  
338 error, the comparison is close to zero [also see Nassar *et al.*, Lopez *et al.*, this issue].

339

340 In addition to the past and present TES CO validation activities reported in this special  
341 Aura validation issue, several sources of CO data have been considered for inter-  
342 comparisons with TES CO retrievals in the near future. These data include CO profile  
343 data from Aqua/AIRS, MLS CO retrievals in the upper troposphere, the upcoming IASI  
344 data set, the long-term MOZAIC measurements, MOPITT data, solar occultation  
345 measurements from the Atmospheric Chemistry Experiment (ACE) Fourier transform  
346 spectrometer [Bernath *et al.*, 2005], and ground-based observations (*e.g.*, Network for the  
347 Detection of Atmospheric Composition Change (NDAAC) data from a global network of  
348 surface sites with longer time coverage). The additional measurement sets will help  
349 validate and confirm the systematic biases in TES tropospheric CO profile relative to the  
350 *in-situ* measurements concluded from this study and Lopez *et al.* (this issue) in the mid-  
351 latitudes and Lopez *et al.* (this issue) in the tropics.

352

353 **Acknowledgments.** Research at the Jet Propulsion Laboratory described in this  
354 paper was performed under contract with the National Aeronautics and Space  
355 Administration.

356

357 Table 1-1. TES and DACOM comparison information for INTEX-B campaign near Houston, March 4 – 21, 2006. Total number of  
 358 DACOM CO profiles for comparisons in 7 flights: 9

	Mar 4		Mar 9		Mar 11	Mar 12		Mar 16	Mar 19		Mar 21
TES Obs Type and RunID	SS 3399		GS 3429		GS 3437	SS 3440		SS 3459	GS 3484		SS 3496
DC-8 Flights	Flt – 3		Flt – 4		Flt – 5	Flt - 6		Flt - 7	Flt – 8		Flt – 9
# of DACOM Profiles	2		2		no coincidence	2		1	2		no coincidence
	Prof 1	Prof 2	Prof 1	Prof 2		Prof 1	Prof 2	Prof 1	Prof 2		
Distance btw TES & DACOM (km)	53	25	24	20		16	16	12	43	88	
Time btw TES & DACOM (hrs)	0.8-1.4	1-1.6	0.5-1.1	0-0.5		0.9-1.25	1-1.5	0-0.5	0-0.3	0.5-1.5	
TES DOF	1.8	1.7	1.3-1.4	1.3-1.4		1.5	1.5	1.5	1.8	1.8	
TES Cloud OD	<0.1	<0.1	<0.1	<0.5		>1.0	<0.1	<0.1-1.0	<0.1	<0.1	

359

360

361

Table 1-2. TES and DACOM comparison information for INTEX-B campaign near Hawaii, April 17 – May 1, 2006. Total number of DACOM CO profiles for comparisons in 5 flights: 15

362

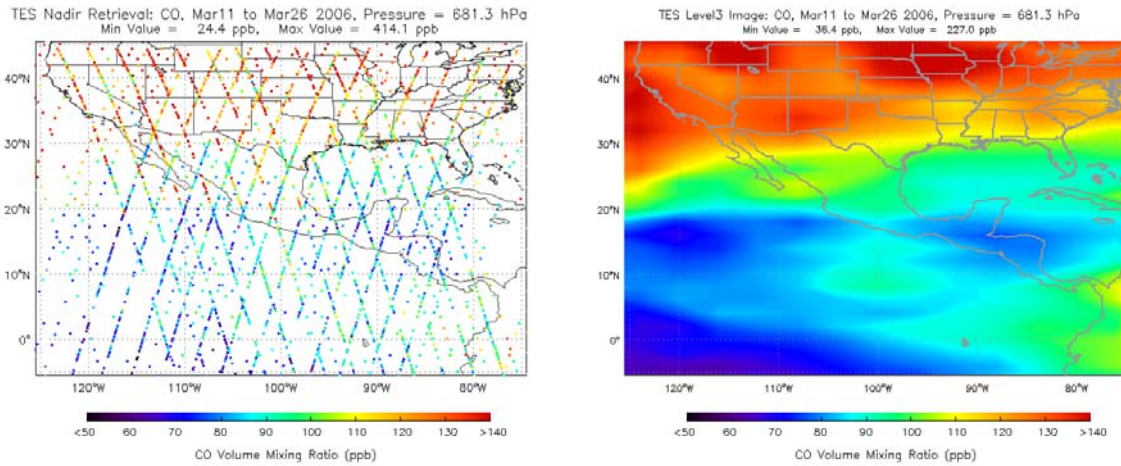
	Apr 17		Apr 23					Apr 25		Apr 28			May 01		
TES Obs Type and RunID	SS 3700		SS 3830					SS 3868		GS 3921			SS 3961		
DC-8 Flights	Flt – 10 (transit)		Flt – 11					Flt – 12		Flt - 13			Flt – 14 (transit)		
# of DACOM Profiles	2		5					2		3			3		
	Prof 1	Prof 2	Prof 1	Prof 2	Prof 1	Prof 2	Prof 3	Prof 1	Prof 2	Prof 1	Prof 2	Prof 3	Prof 1	Prof 2	Prof 3
Distance btw TES & DACOM (km)	17	328	45	21	23	23	15	37	20	6	60	4	96	18	102
Time btw TES & DACOM (hrs)	0-0.5	0.5-1.2	1.8-2.3	0.5-1.2	0-0.5	1-1.5	1.7-2.2	2.5-3.0	0-0.3	1.5-2.0	0.5-1.2	0-0.3	5-6	1.0-1.5	0-0.5
TES DOF	1.6	1.4	1.6	1.5-1.7	1.5-1.6	1.5-1.6	1.0-1.5	1.4-1.5	1.2-1.3	1.6	1.7	1.1	1.3-1.6	1.0-1.3	0.2-0.7
TES Cloud OD	<0.1	<0.1	<0.1 & 0.7	<0.1 & 1.0	<0.1 – 1.4	<0.1	<0.1 & 3.0	<0.1 & 0.7	<0.1 & 0.4	<0.1	<0.1	2.3	<0.1 & 2	0.9-2.0	1.7-4.0

363

364 Table 1-3. TES and DACOM comparison information for INTEX-B campaign near  
 365 Anchorage, May 4– 15, 2006. Total number of DACOM CO profiles for comparisons in  
 366 5 flights: 3

	May 04	May 07	May 09	May 12	May 15
TES Obs Type and RunID	GS	SS 4112	SS 4154	GS 4211	SS 4268
DC-8 Flights	Flt – 15	Flt – 16	Flt – 17	Flt – 18	Flt – 18 (transit)
# of DACOM Profiles	no coincidence	1	1	1	no coincidence
Distance btw TES & DACOM (km)		322	10	176	
Time btw TES & DACOM (hrs)		1.5-2.0	1.5-2.0	0-0.5	
TES DOF		1.3-1.5	1.2-1.5	1.1	
TES Cloud OD		<0.1 & 0.4	<0.1 & 1.2	0.5	

367



368

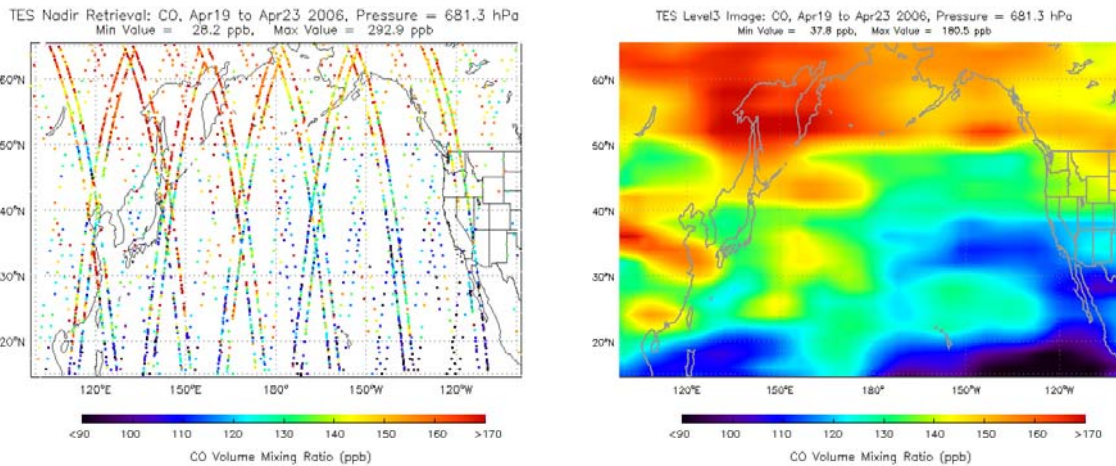
369

370 Figure 1. TES Global Survey and Step & Stare observations of CO near Houston, March  
371 11 to 26, 2006. The pressure level plotted is 681.3 hPa. The left panel shows the  
372 enlarged footprints (size of the real footprint is 8.3X5.3 km). The right panel shows the  
373 bin-averaged image with the bin size of 6° longitude X 1.6° latitude.

374

375

376



377

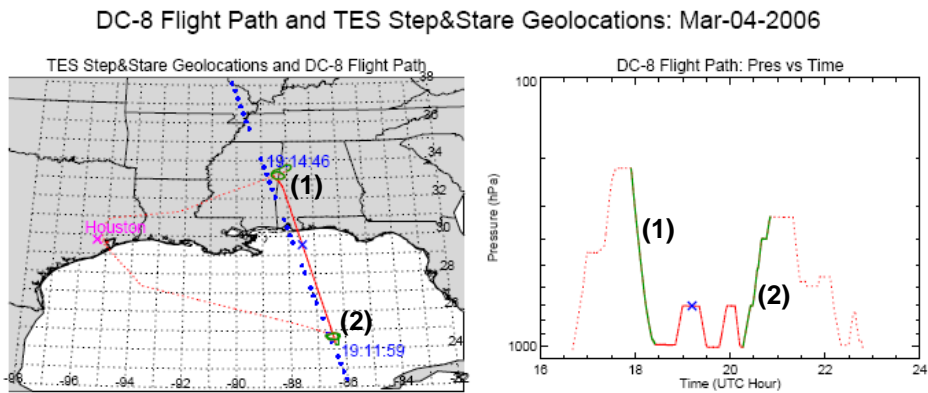
378

379 Figure 2. TES Global Survey and Step & Stare observations of CO over Pacific Ocean,  
380 April 19 to 23, 2006. Plotting methodology is identical to Figure 1.

381

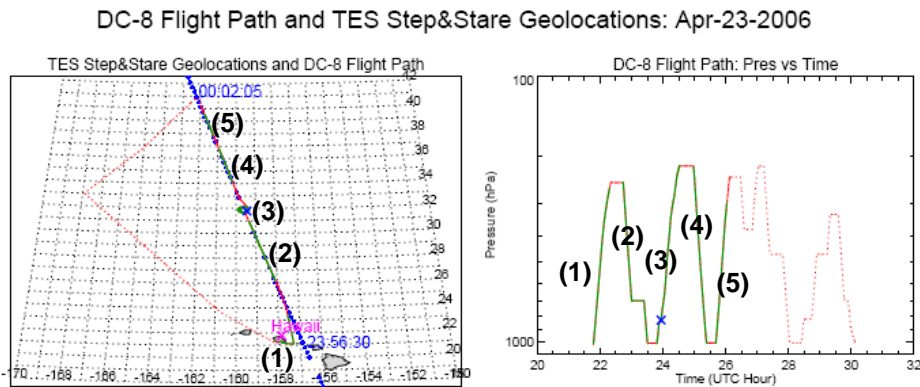
382

383  
384  
385  
386  
387  
388  
389  
390  
391



392 Figure 3. Left panel shows DC-8 flight path (red) and TES Step&Stare geolocations (blue  
393 dots) for March 4, 2006 near Houston. The right panel shows the DC-8 flight path in  
394 pressure as a function of UTC time. The blue cross symbols are where and when DC-8  
395 and TES coincide in time, and the green lines represent the two selected DC-8 vertical  
396 spirals through the atmosphere. The DACOM CO measurements taken in these two  
397 spiral profiles are used for TES validation.

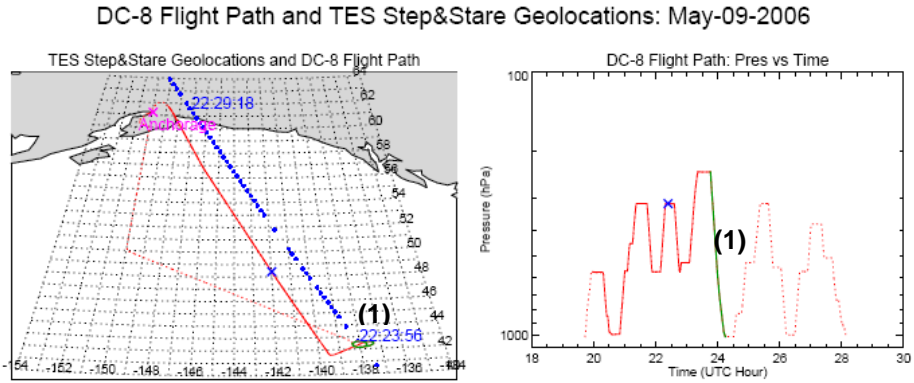
398  
399  
400  
401



402  
403  
404  
405  
406  
407  
408  
409  
410  
411  
412  
413

410 Figure 4. DC-8 flight path and TES Step&Stare geolocations for April 23, 2006 near  
411 Hawaii. All symbols and colored lines are the same as those in Figure 3. The DACOM  
412 CO measurements taken in the four spiral and one departure profiles are used for TES  
413 validation.

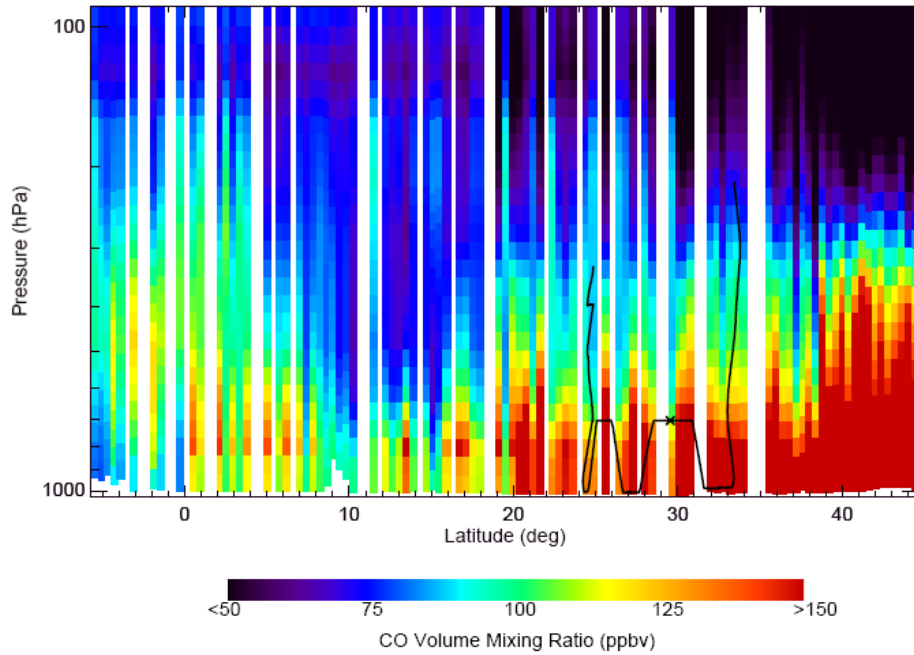
414  
415  
416  
417  
418  
419  
420  
421  
422



423 Figure 5. DC-8 flight path and TES Step&Stare geolocations for May 9, 2006 near  
424 Anchorage. All symbols and colored lines are the same as those in Figure 3. The  
425 DACOM CO measurements taken in the spiral profile are used for TES validation.  
426

427  
428

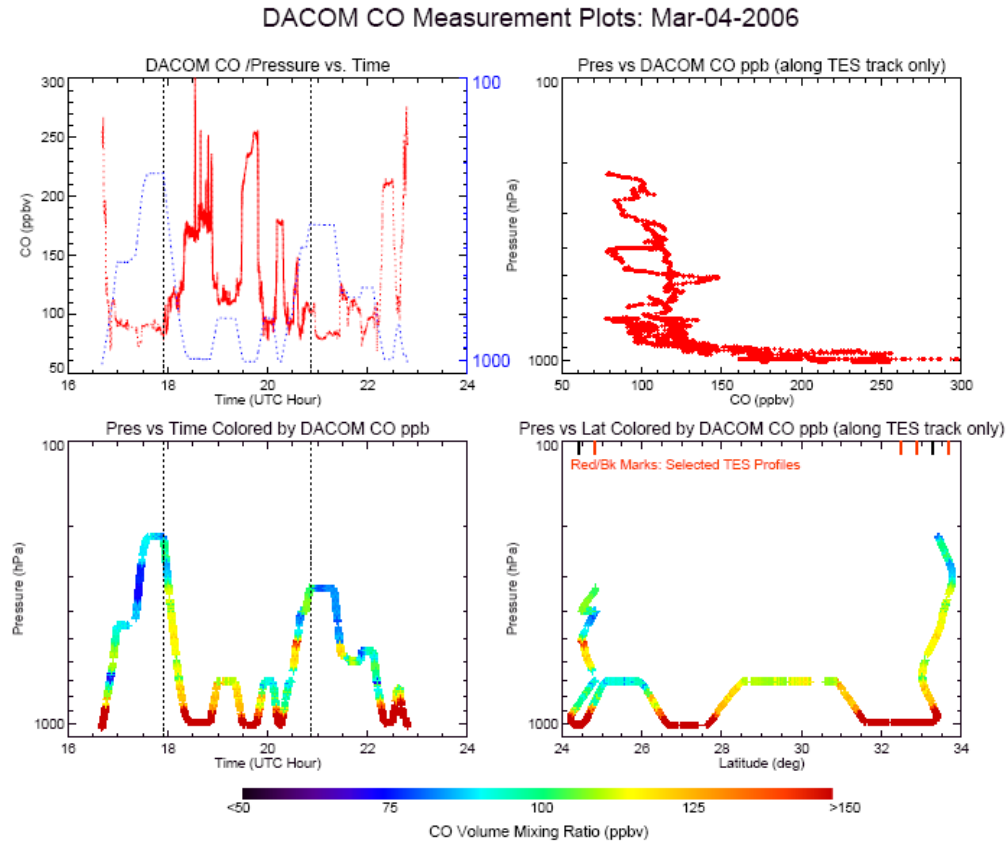
429 **TES Step & Stare Nadir Retrieval Result: CO**  
Cross Section Along Orbit Track, Run=3399, Seq=1-1, Scan = 0-124, UTtime=Mar-04-2006 19:03-19:17



430  
431  
432  
433  
434  
435  
436  
437  
438  
439  
440  
441  
442

443 Figure 6. Along satellite ground track latitude vs. pressure curtain plot for TES CO  
444 retrievals taken in the Step & Stare observation run in March 4, 2006, near Houston (see

445 Figure 1 for geolocations of the measurements). The DC-8 flight path pressure values are  
 446 shown in black and the symbol X indicates the location where TES and DC-8 coincide in  
 447 time.  
 448  
 449



450  
 451  
 452 Figure 7. DACOM CO plots for the March 4, 2006 flight near Houston. Shown are the  
 453 CO values as a function of time overlaid with the pressure of the DC-8 aircraft (upper left  
 454 panel), the CO values as a function of pressure for the aircraft path overlap with TES  
 455 geolocations (upper right panel), the CO values as a function of time and pressure (lower  
 456 left panel), and the CO values as a function of latitude and pressure (lower right panel).  
 457 This last panel can be compared to the TES curtain plot (figure 6). The red/black marks  
 458 at the top of the lower-right panel are the TES profile locations used to compare with the  
 459 two DACOM CO profiles, respectively (black being the TES profile closest in distance to  
 460 the averaged DACOM locations).  
 461

462

DACOM CO (red) and TES CO Interpolated to DC-8 Track (blue): Mar-04-2006

463

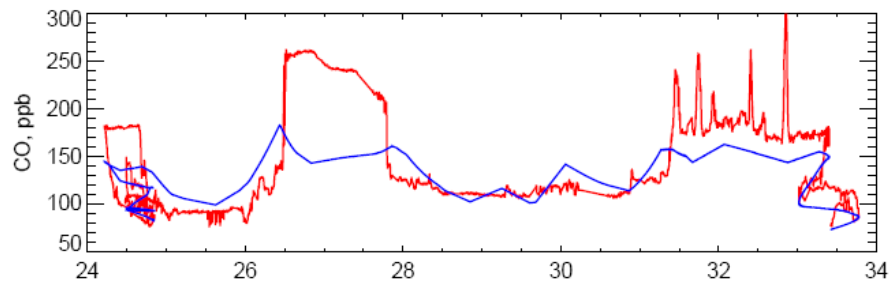
464

465

466

467

468



469

470

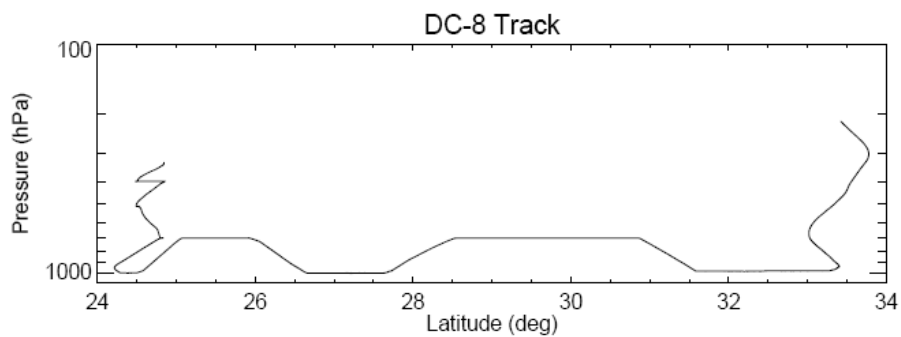
471

472

473

474

475



476

477 Figure 8. TES-retrieved CO values are interpolated spatially to the DC-8 flying path (blue

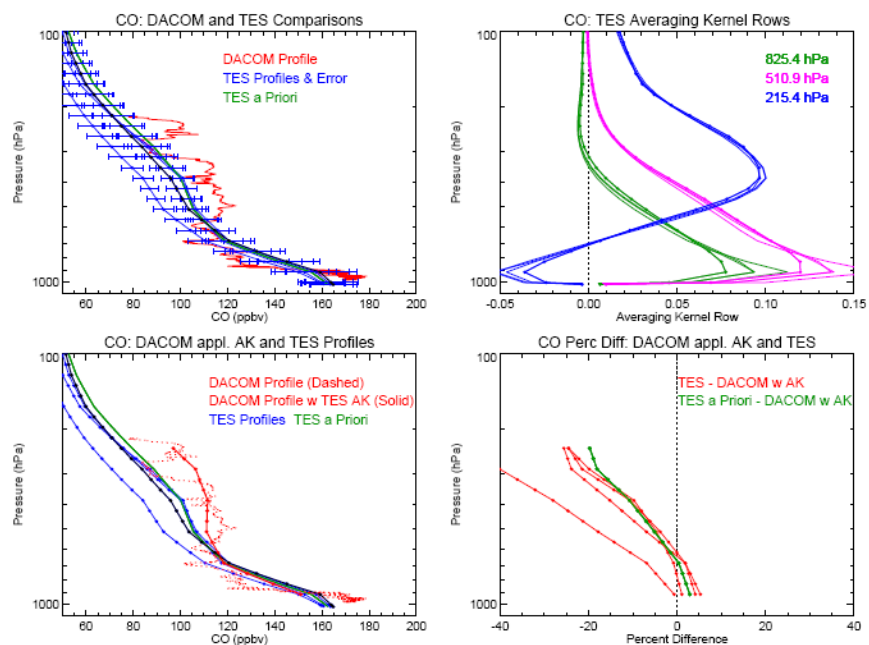
478 line) and compared to DACOM CO values measured by (red line) (upper panel). The

479 DC-8 pressures as a function of latitude are shown in the lower panel.

480

481

TES & DACOM CO Comparisons (1): Mar-04-2006



482

483 Figure 9. An example of TES and DACOM CO profile comparisons. The CO profiles  
 484 were taken near Houston, March 4, 2006. The DACOM CO values (red in upper and  
 485 lower left panels) were sampled in the spiral down flight portion (figure 3, profile (1)).  
 486 Four TES CO profiles near the DACOM profile are selected for comparisons (blue/black  
 487 in upper and lower left panels, the black profile being the one closest to the averaged  
 488 DACOM locations in distance). The TES averaging kernels (AK) corresponding to three  
 489 sample pressures are plotted in upper right panel. The lower right panel shows the  
 490 percent difference in CO profiles between TES and DACOM, where the DACOM profile  
 491 is the one after applying TES AK and the *a priori* profile.

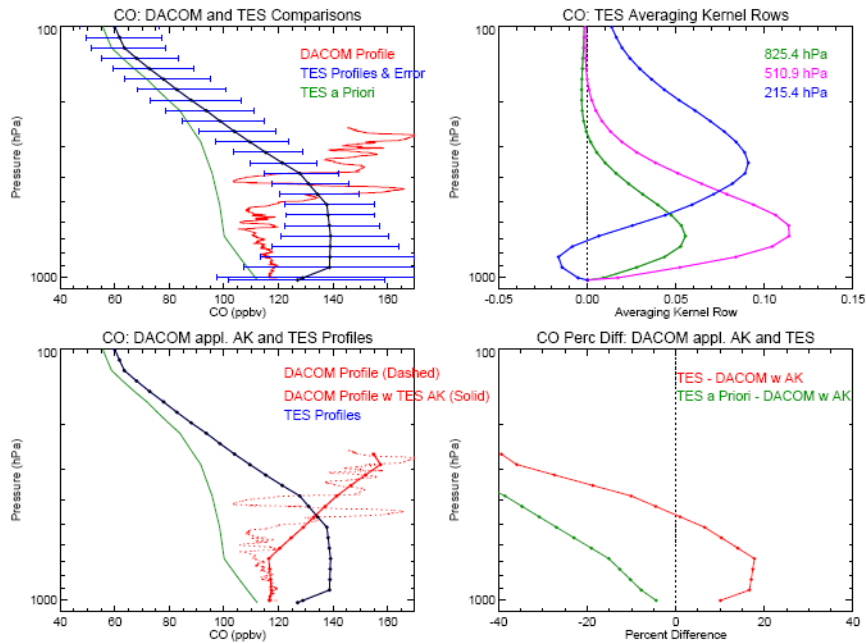
492

493

494

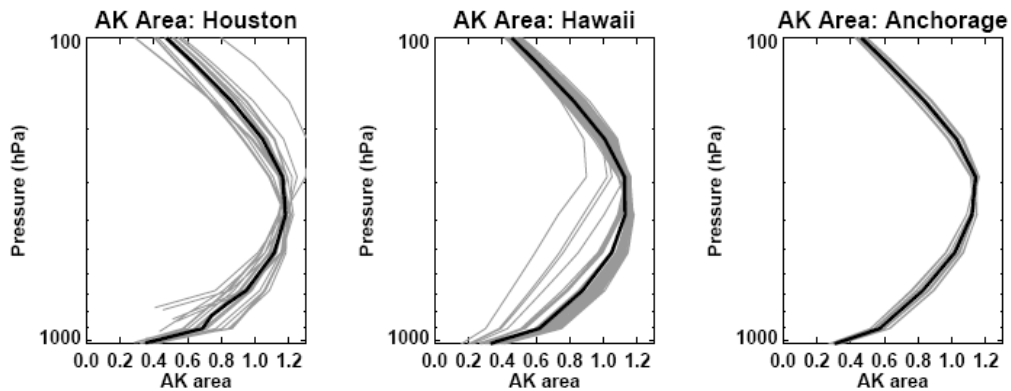
495

TES & DACOM CO Comparisons (1): Apr-28-2006



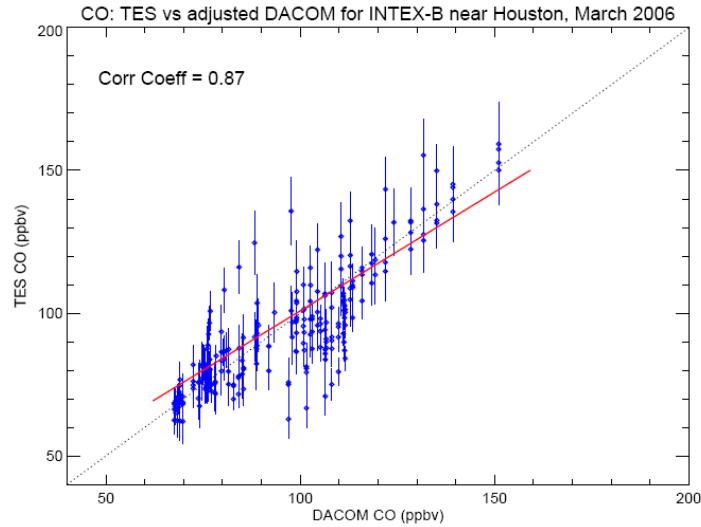
496  
497  
498  
499  
500  
501

Figure 10. Similar to Figure 9, another example of TES and DACOM CO profile comparisons. The TES and DACOM CO profiles were taken near Hawaii, April 28, 2006.



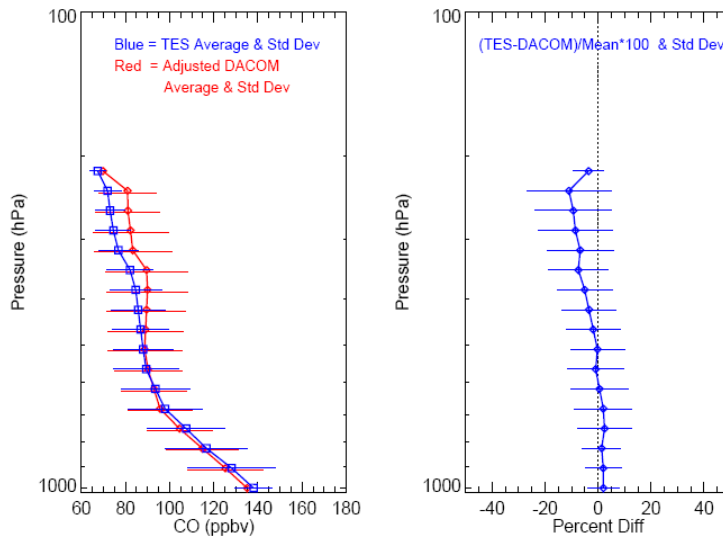
502  
503  
504  
505  
506  
507

Figure 11. The area of the averaging kernels as a function of pressure for the selected TES CO profiles used to compare with DACOM in-situ profiles near Houston, Hawaii, and Anchorage regions. The individual profiles are in light gray and the averaged profiles are in black for the three regions respectively.



508

CO: TES and Adjusted DACOM Comparison for INTEX-B near Houston, March 2006



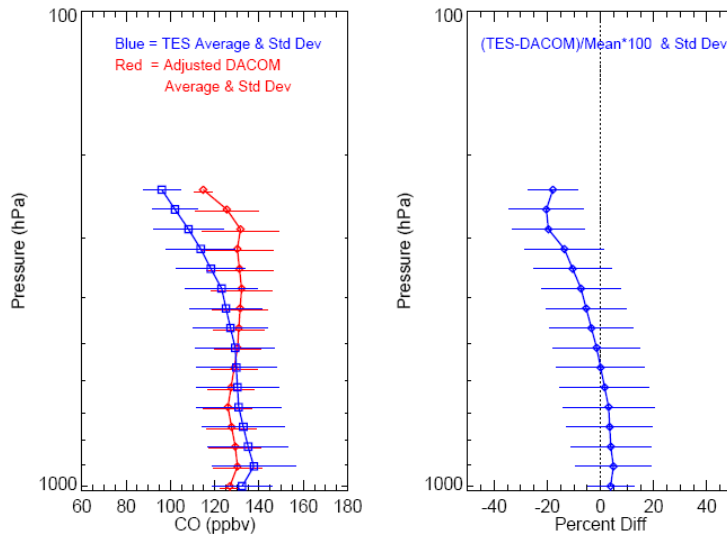
509

510

511

512 Figure 12. Summary plots for TES and DACOM CO profile comparisons during  
 513 INTEX-B near Houston, March 2006. The top panel shows the correlation plot of TES  
 514 with retrieval error vs. DACOM CO profiles, where DACOM CO profiles are those with  
 515 TES AK and *a priori* profiles applied (see the example in Figure 9). The bottom-left  
 516 panel shows the averaged CO profiles of TES and DACOM with standard deviations  
 517 (vertically shifted for distinguishing) from the two measurement sets. The bottom-right  
 518 panel shows the averaged percent differences between TES and DACOM CO profiles  
 519 with the standard deviation.

CO: TES and Adjusted DACOM Comparison for INTEX-B near Hawaii, April 2006



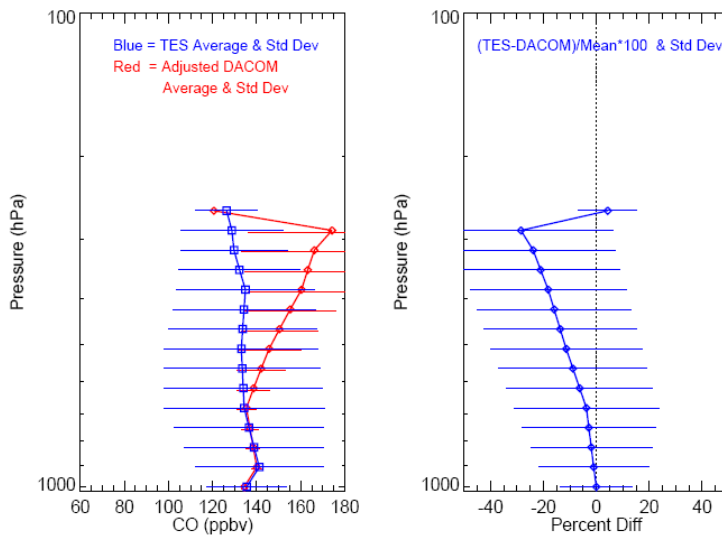
520

521

522 Figure 13. Summary plots for TES and DACOM CO profile comparisons during  
523 INTEX-B near Hawaii, Apr-May 2006. All the colored symbols and lines are defined  
524 the same as in Figure 12.

525

CO: TES and Adjusted DACOM Comparison for INTEX-B near Anchorage, May 2006



526

527

528 Figure 14. Summary plots for TES and DACOM CO profile comparisons during  
529 INTEX-B near Anchorage, May 2006. The colored symbols and lines are defined the  
530 same as in Figure 12.

531 **References**

532

533 Beer, R., T. A. Glavich, and D. M. Rider (2001), Tropospheric Emission Spectrometer  
534 for the Earth Observing System Aura satellite, *Appl. Opt.*, *40*, 2356-2367.

535

536 Beer, R. (2006), TES on the Aura mission: scientific objectives, measurements, and  
537 analysis overview, *IEEE Transact. Geosci. Remote Sens.*, *44*, 1102-1105.

538

539 Bernath et al. (2005), Atmospheric Chemistry Experiment (ACE): Mission overview,  
540 *Geophys. Res., Lett.*, *32*, L15S01, doi:10.1029/2005GL022386.

541

542 Clerbaux, C., J. Gille, and D. Edwards (2004), Infrared measurements of atmospheric  
543 pollution from space. *Atmospheric Environment*, *38*:4599-4601.

544

545 Emmons, L. K., M. N. Deeter, J. C. Gille, D. P. Edwards, J.-L. Attie, J. Warner, D.  
546 Ziskin, G. Francis, B. Khattatov, V. Yudin, J.-F. Lamarque, S.-P. Ho, D. Mao, J. S. Chen,  
547 J. Drummond, P. Novelli, G. Sachse, M. T. Coffey, J. W. Hnnigan, C. Gerbig, S.  
548 kawakami, Y. Kondo, N. Takegawa, H. Schlager, J. Baehr, and H. Ziereis (2004),  
549 Validation of Measurements of Pollution in the Troposphere (MOPITT) CO retrievals  
550 with aircraft in situ profiles, *J. Geophys. Res.*, *109*, D03309, doi:10.1029/2003JD004101.

551

552 Heald, C.L., D.J. Jacob, A.M. Fiore, L.K. Emmons, J.C. Gille, M.N. Deeter, J. Warner,  
553 D.P. Edwards, J.H. Crawford, A.J. Hamlin, G.W. Sachse, E.V. Browell, M.A. Avery,  
554 S.A. Vay, D.J. Westberg, D. R.Blake, H.B.Singh, S.T. Sandholm, R.W. Talbot, H.E.  
555 Fuelberg (2003), Asian outflow and transpacific transport of carbon monoxide and ozone  
556 pollution: An integrated satellite, aircraft and model perspective, *J. Geophys. Res.-*  
557 *Atmos.*, *108* (D24), 4804, doi:10.1029/2003JD003507.

558

559 Kulawik, S.S, J. Worden, A. Eldering, K.W. Bowman, M. Gunson, G. Osterman, L.  
560 Zhang, D. Jacob, S.A. Clough, M. Shephard, R. Beer (2006), Implementation of Cloud  
561 Retrievals for Tropospheric Emission Spectrometer (TES) Atmospheric Retrievals - part I  
562 description and characterization of errors on trace gas retrievals, *J. Geophys. Res.-Atmos.*,  
563 *111*, D24204, doi:10.1029/2005JD006733.

564

565 Livesey, N. et al., Validation of EOS Microwave Limb Sounder O3 and CO observations  
566 in the upper troposphere and lower stratosphere, *J. Geophys. Res.-Atmos.*, submitted,  
567 2007.

568

569 Logan, et al. (1981), Tropospheric chemistry: A global perspective, *J. Geophys. Res.*, *86*,  
570 7210-7254.

571

572 Lopez, J. et al., TES carbon monoxide validation during two AVE campaigns using the  
573 Argus and ALIAS instruments on NASA's WB-57F, *J. Geophys. Res.-Atmos.*, submitted,  
574 2007.

575

576 Luo, M., C. P. Rinsland, C. D. Rodgers, J. A. Logan, H. Worden, S. Kulawik, A.  
577 Eldering, A. Goldman, M. W. Shephard, M. Gunson, and M. Lampel (2007), Comparison  
578 of carbon monoxide measurements by TES and MOPITT - the influence of a priori data  
579 and instrument characteristics on nadir atmospheric species retrievals, *J. Geophys. Res.*,  
580 *112*, D09303, doi:10.1029/2006JD007663..  
581  
582 Luo, M., N. Richards, G. Osterman, S. Kulawik, and the TES team, Tropospheric Ozone  
583 and CO monthly mean fields from TES and GEOS- CHEM model, AGU Fall Meeting,  
584 December 2006 (available at <http://tes.jpl.nasa.gov/docsLinks/presentations.cfm>).  
585  
586 Nassar, R. J. A. Logan, H. Worden, I. A. Megretskaia, Validation of Tropospheric  
587 Emission Spectrometer (TES) Nadir Ozone Profiles Using Ozone-sonde Measurements,  
588 submitted, *J. Geophys. Res.*, submitted, 2007.  
589  
590 Rinsland, C. P., M. Luo, J. A. Logan, R. Beer, H. M. Worden, J. R. Worden, K. Bowman,  
591 S. S. Kulawik, D. Rider, G. Osterman, M. Gunson, A. Goldman, M. Shephard, S. A.  
592 Clough, C. Rodgers, M. Lampel, and L. Chiou (2006), Nadir measurements of Carbon  
593 Monoxide (CO) distributions by the Tropospheric Emission Spectrometer instrument  
594 onboard the Aura spacecraft: Overview of analysis approach and examples of initial  
595 results, *Geophys. Res. Lett.*, Vol. 33, No. 22, L22806.10.1029/2006GL027000.  
596  
597 Rodgers, C. D. (2000), *Inverse Methods for Atmospheric Sounding: Theory and Practice*,  
598 World Sci., River Edge, N. J.  
599  
600 Rodgers, C. D., and B. J. Connor (2003), Intercomparisons of remote sounding  
601 instruments, *J. Geophys. Res.*, *108*, 4116, doi:10.1029/2002JD002299.  
602  
603 Osterman, G. *et al.* (2006), Tropospheric emission spectrometer (TES) validation report,  
604 JPL D33192, version 2.0 (available at <http://tes.jpl.nasa.gov/docsLinks/documents.cfm>).  
605  
606 Sachse, G. W., G. F. Hill, L. O. Wade, and M. G. Perry (1987), Fast-response, high-  
607 precision carbon monoxide sensor using a tunable diode laser absorption technique, *J.*  
608 *Geophys. Res.*, *92*, 2071-2081.  
609  
610 Shephard, M. W., H. M. Worden, K. E. Cady-Pereira, S. A. Clough, D. M. Rider, D. C.  
611 Tobin, H. E. Revercomb, H. H. Aumann, M. Lampel, B. M. Fisher, K. W. Bowman, E.  
612 Sarkissian, D. Tremblay, M. Gunson, R. Beer, M. Luo, G. B. Osterman Tropospheric  
613 Emission Spectrometer Spectral Radiance Comparisons, *J. Geophys. Res.*, submitted,  
614 2007.  
615  
616 Worden, H.M., J. Logan, J. R. Worden, R. Beer, K. Bowman, S. A. Clough, A. Eldering,  
617 B. Fisher, M. R. Gunson, R. L. Herman, S. S. Kulawik, M. C. Lampel, M. Luo, I. A.  
618 Megretskaia, G. B. Osterman, and M. W. Shephard (2007), Comparisons of Tropospheric  
619 Emission Spectrometer (TES) ozone profiles to ozone-sondes: Methods and initial results,  
620 *J. Geophys. Res.*, *112*, D03309, doi:10.1029/2006JD007258.  
621